Rayleigh-Plesset equation of the bubble stable cavitation in water: A nonequilibrium all-atom molecular dynamics simulation study

Viet Hoang Man, Mai Suan Li, Philippe Derreumaux, and Phuong H. Nguyen

Citation: The Journal of Chemical Physics **148**, 094505 (2018); doi: 10.1063/1.5009910
View online: https://doi.org/10.1063/1.5009910
View Table of Contents: http://aip.scitation.org/toc/jcp/148/9
Published by the American Institute of Physics

Rayleigh-Plesset equation of the bubble stable cavitation in water: A nonequilibrium all-atom molecular dynamics simulation study

Viet Hoang Man,[1] Mai Suan Li,[2,3] Philippe Derreumaux,[4] and Phuong H. Nguyen[4,a)]
[1]*Department of Physics, North Carolina State University, Raleigh, North Carolina 27695-8202, USA*
[2]*Institute of Physics, Polish Academy of Sciences, Al. Lotnikow 32/46, 02-668 Warsaw, Poland*
[3]*Institute for Computational Sciences and Technology, SBI building, Quang Trung Software City, Tan Chanh Hiep Ward, District 12, Ho Chi Minh City, Vietnam*
[4]*Laboratoire de Biochimie Théorique UPR 9080, CNRS, Université Denis Diderot, Sorbonne Paris Cité IBPC, 13 Rue Pierre et Marie Curie, 75005 Paris, France*

(Received 20 October 2017; accepted 16 February 2018; published online 6 March 2018)

The Rayleigh-Plesset (RP) equation was derived from the first principles to describe the bubble cavitation in liquids in terms of macroscopic hydrodynamics. A number of nonequilibrium molecular dynamics studies have been carried out to validate this equation in describing the bubble inertial cavitation, but their results are contradictory and the applicability of the RP equation still remains to be examined, especially for the stable cavitation. In this work, we carry out nonequilibrium all-atom simulation to validate the applicability of the RP equation in the description of the stable cavitation of nano-sized bubbles in water. We show that although microscopic effects are not explicitly included, this equation still describes the dynamics of subnano-bubbles quite well as long as the contributions of various terms including inertial, surface tension, and viscosity are correctly taken into account. These terms are directly and inversely proportional to the amplitude and period of the cavitation, respectively. Thus, their contributions to the RP equation depend on these two parameters. This may explain the discrepancy between the current results obtained using different parameters. Finally, the accuracy of the RP equation in the current mathematical modeling studies of the ultrasound-induced blood-brain-barrier experiments is discussed in some detail. *Published by AIP Publishing.*
https://doi.org/10.1063/1.5009910

I. INTRODUCTION

A bubble in liquids is a spherical volume of gas. It may undergo oscillations in size if subjected to external forces. If the oscillation is slow, then the contraction and expansion of size are approximately symmetric. This phenomenon, called stable cavitation, produces rapid flows of liquid around the bubble and induces shear stress on nearby objects. In contrast, a fast oscillation may lead to asymmetric contraction and expansion followed by a violent collapse called inertial cavitation. The well-known equation that describes the bubble dynamics in terms of hydrodynamics is the so-called generalized Rayleigh-Plesset (RP) equation,[1–7]

$$p_g(R,t) = \rho\left\{R\ddot{R} + \frac{3}{2}\dot{R}^2\right\} + p_\infty + \frac{2\gamma_\infty}{R}\left(1 - \frac{\delta_T}{R}\right) + \frac{4\eta_\infty \dot{R}}{R}\left(1 + \frac{\delta_{vis}}{R}\right)^{-1}, \quad (1)$$

where $\dot{R}$ and $\ddot{R}$ represent respectively the first- and second-order time derivatives of the bubble radius $R(t)$, $p_g(R, t)$ is the pressure in the bubble, p_∞ is the pressure in the liquid at a large distance from the bubble, and ρ is the liquid mass density. The first part of this equation was originally derived by Lord Rayleigh and Plesset.[1,2] Then, the surface tension constant of the bubble, γ_∞, was added by Noltingk and Neppiras,[3,4] and the coefficient of the viscosity of the bulk liquid, η_∞, was introduced by Poritsky.[5] The first-order curvature corrections in the surface tension and viscosity were later suggested by Dzubiella via the empirical coefficients δ_T[6] and δ_{vis},[7] respectively. Neglecting liquid compressibility effects, this equation can be derived entirely from first principles using the bubble radius as the dynamics parameter[8] or from the Navier-Stokes equations under the assumption of spherical symmetry.[9]

Because the RP equation is a continuum hydrodynamics equation, it should describe well the dynamics of bubbles from a macroscopic point of view, which is indeed verified by numerous experiments.[10] However, in general, each physical phenomenon has its own scale below which equations of continuum hydrodynamics maybe not fulfilled. In this context, it is unclear whether the RP equation is applicable to describe dynamics of nanoscale or microscale bubbles. Experimental investigation is technically very difficult due to fragility of bubbles,[11] and in addition bubbles with radii $\lesssim$10 nm are not available for experimental studies. As a remedy, a number of nonequilibrium molecular dynamics (NEMD) simulations have been carried out to verify the RP equation for nano-bubbles. Here, a bubble is formed by heating or removing some liquid molecules, creating an empty space in the liquid. It is then compressed by surrounding molecules during the simulation, mimicking the bubble collapse. This way, Okumura and Ito showed that the formation and collapse of a nano-bubble in liquid argon are well described by the RP equation.[12] Holyst

a)Email: phuong.nguyen@ibpc.fr

and colleagues confirmed this result by large-scale NEMD simulations of nano-bubbles with radii ranging from 5 to 12 nm in liquid argon despite the nonuniform profile of the pressure in the liquid.[13,14] Mao and Zhang, however, showed that the RP equation leads to negative surface tension of bubbles in water, implying the invalidity of the RP equation.[15] Dzubiella showed that the effect of water viscosity due to high curvatures of the nano-bubble surface has to be corrected such that the RP equation can describe correctly simulation data.[7] The effects of temperature and ionic condition on the collapse of bubbles in water were also simulated by Lugli and colleagues.[16,17] The goal of this work is to verify the RP equation to describe the *stable cavitation of subnano-bubbles* ($\lesssim$1 nm); we compare the inner bubble pressure, $p_g(R, t)$, calculated directly from simulation data with that calculated by the RP equation [Eq. (1)]. This is important because all current NEMD simulations only study the inertial cavitation, and it is of fundamental interest to understand whether the RP equation is also valid for the stable cavitation. Furthermore, the stable cavitation has a wide range of applications in emerging important fields such as ultrasound-induced blood-brain-barrier opening for drug delivery[18] and activating neuronal activity.[19] Mathematical modeling of these experiments is largely based on the RP equation,[20–25] and thus it is urgent to verify the RP equation to assess the levels of accuracy of theories.

II. THEORY AND SIMULATION

A. The bubble model and inner pressure

Recently, we have developed a method to simulate the bubble stable cavitation in water.[26] It is useful to briefly summarize the main aspects of the bubble model here. A bubble is represented by a particle with low mass and no charge, and interacts with surrounding waters by a time-dependent Lennard-Jones potential,

$$V[r, \sigma(t)] = 4\epsilon\Big[\Big(\frac{\sigma(t)}{r}\Big)^{12} - \Big(\frac{\sigma(t)}{r}\Big)^{6}\Big], \tag{2}$$

where r is the distance between the center of the bubble and the oxygen atom or the hydrogen atoms of a water molecule, $R(t) \equiv \sigma(t)$ is the bubble radius, and ϵ is a parameter which is large enough such that the repulsive part is hard enough, but simulations are still stable. We found that the results do not depend much on the value of ϵ, and in practice, we simply set ϵ about ten times larger than that of the water-water interaction. To mimic the stable expansion and contraction of the bubble, the time-dependent bubble radius is expressed as a sinusoidal function,

$$R(t) = \frac{(R_{\max} + R_{\min})}{2} + \frac{(R_{\max} - R_{\min})}{2}\cos\Big(\frac{2\pi t}{\tau} + \pi\Big), \tag{3}$$

where τ is the vibrational period of the bubble radius. The radius of the bubble varies between $R_{\min}$ at $t = n\tau$ and $R_{\max}$ at $t = (n + 1/2)\tau$, where $n = 0, 1, 2, 3, \ldots$ is the periodicity. This way, the time-dependent potential [Eq. (2)] changes harmonically during the simulation, mimicking the stable cavitation. We should mention that the low mass of the bubble particle facilitates the translation of the bubble to everywhere in the system, mimicking the experimental situation.

The velocity and acceleration of the bubble radius are time derivatives of the radius and given by

$$\begin{aligned}\dot{R}(t) &= -\pi\frac{(R_{\max} - R_{\min})}{\tau}\sin\Big(\frac{2\pi t}{\tau} + \pi\Big),\\ \ddot{R}(t) &= -2\pi^2\frac{(R_{\max} - R_{\min})}{\tau^2}\cos\Big(\frac{2\pi t}{\tau} + \pi\Big).\end{aligned} \tag{4}$$

Because of the presence of the dispersion interaction between the bubble and solvent [Eq. (2)], the RP equation is modified to include this term as shown by Dzubiella,[6,7]

$$\begin{aligned}p_g(R, t) = \rho\Big\{R\ddot{R} + \frac{3}{2}\dot{R}^2\Big\} + p_\infty + \frac{2\gamma_\infty}{R}\Big(1 - \frac{\delta_T}{R}\Big)\\ + \frac{4\eta_\infty\dot{R}}{R}\Big(1 + \frac{\delta_{vis}}{R}\Big)^{-1} - \rho_0 V(R),\end{aligned} \tag{5}$$

where $V(R)$ is the dispersion interaction between the bubble particle and a solvent molecule, and ρ_0 is the liquid number density.

Unlike real filled gas bubbles, there exist no gas molecules in the interior of our model. Instead, the Lennard-Jones potential [Eq. (2)] maintains the mechanical stability of the bubble and acts as an encounter to the collisional force that an impinging water exerts on the bubble surface. Therefore, the inner pressure can be calculated from the reversed momentum of the colliding water molecules on the bubble surface. Based on this argument, Takahashi and colleague have developed a simple method to calculate the inner bubble pressure from the bubble-water radial distribution function (RDF) $g_{bw}(R, t)$ as follows:[27]

$$p_g(R, t) \approx \rho g_{bw}(R, t) k_B T, \tag{6}$$

where k_B is the Bolztmann constant, T is the temperature, and R is the position of the first peak of g_{bw} at time t. For small bubbles which are surrounded by a few waters, the calculation via g_{bw} provides better statistics than the conventional method using the virial expression. We note that because in our model the bubble particle only interacts with the water oxygen atoms, g_{bw} is actually the radial distribution between water oxygen atoms and the bubble.

B. Simulation details

Using this bubble model, we carried out NEMD simulations for a single bubble centered in a cubic box with an edge of L = 8 nm, containing ≈8000 TIP3P waters at 300 K. Two cases where the bubble undergoes large ($R_{\min}$ = 0.3 nm, $R_{\max}$ = 0.9 nm) and small ($R_{\min}$ = 0.3 nm, $R_{\max}$ = 0.4 nm) cavitation amplitudes are simulated. The cavitation period τ = 50 ps is used in all calculations. For each case, 100 NEMD trajectories, each 100 ps long, starting from different initial water structures selected from a short 1 ns equilibrium MD trajectory are carried out. The GROMACS program[28] coupled to our code for simulating bubble vibration is employed. The bond lengths with hydrogen atoms are fixed with the SHAKE algorithm,[29] and the equations of motion are integrated with a time step of 0.2 fs using the leapfrog algorithm. Note that this small step is necessary to maintain the stability of the simulations. The electrostatic interactions are calculated using the particle mesh Ewald method and a cutoff of 1.2 nm.[30] A cutoff of 1.2 nm is used for the van der Waals interaction between

water-water, and a time-dependent cutoff, which is equal to the bubble radius $R(t)$ [Eq. (3)], is used for the van der Waals interaction between water molecules and the bubble. This guarantees that the bubble interacts only with water molecules on the bubble surface. The nonbonded pair lists are updated every 10 fs. The system volume and temperature are maintained at equilibrium using the Berendsen coupling procedures.[31] Using the same procedure, we carried out additionally one NEMD simulation of a system with a large box size of $L = 21$ nm, containing 188 354 waters, and all other parameters are the same for the small system.

III. RESULTS

Our aim is to validate the RP equation via the comparison of the inner bubble pressure $p_g(R, t)$ calculated directly from simulation with that calculated by the RP equation [Eq. (5)]. In particular, we study the contributions of the inertial term, the surface tension, and the viscosity to the accuracy of the RP equation. In the following, we present results of two cases where the bubble undergoes large ($R_{\min} = 0.3$ nm, $R_{\max} = 0.9$ nm) and small ($R_{\min} = 0.3$ nm, $R_{\max} = 0.4$ nm) cavitation amplitudes. The cavitation period $\tau = 50$ ps is used in all calculations. This period is chosen because of two main reasons. First, it is short enough such that we can perform multiple simulations within a time scale of picoseconds, which is 100 ps in this work (we can capture two periods). For short periods, say $\tau \leq 10$ ps, the simulations are usually unstable because fast changes take place in the system. Second, as shown below, the results depend on the ratio $\Delta R/\tau$ ($\Delta R \equiv R_{\max} - R_{\min}$) [Eq. (4)]; thus, it is sufficient to fix one parameter (in this case, we fix $\tau = 50$ ps) and study the influence of another parameter on the RP equation.

A. Bubble dynamics

During the bubble cavitation, waters are pushed back and forth and redistributed around the bubble. As seen from Fig. 1(a), the radial distribution function (RDF) between the bubble and waters, $g_{\rm bw}(r)$, is flat at 25 ps when the bubble is fully expanded and exhibits a sharp peak at 50 ps when the bubble is fully compressed. In both cases, the distribution is vanished at distances smaller than the bubble radius, indicating that the Lennard-Jones potential [Eq. (2)] is hard enough to prevent the access of waters into the bubble interior. Although the radius of the bubble is theoretically defined by Eq. (3), it is more appropriate to take into account the surface thickness to mimic real bubbles. To this end, we consider the first solvation shell as the bubble surface and define the bubble effective radius as the position of the first peak of $g_{\rm bw}(r)$. We calculate $g_{\rm bw}(r)$ at different time steps along the nonequilibrium trajectories and identify the position of the first peaks whose time-evolution is shown in Fig. 1 [(b), green curve]. As seen, the effective radius behaves like its counterpart defined by Eq. (3) (orange curve), but it shifted upward by ~0.15 nm. We fit these data to a function of the form of Eq. (3) and obtain $R_{\min} = 0.43$ nm and $R_{\max} = 1.12$ nm. To reveal the bubble dynamics, we calculate analytically the first (velocity) and second (acceleration) time derivatives of the bubble

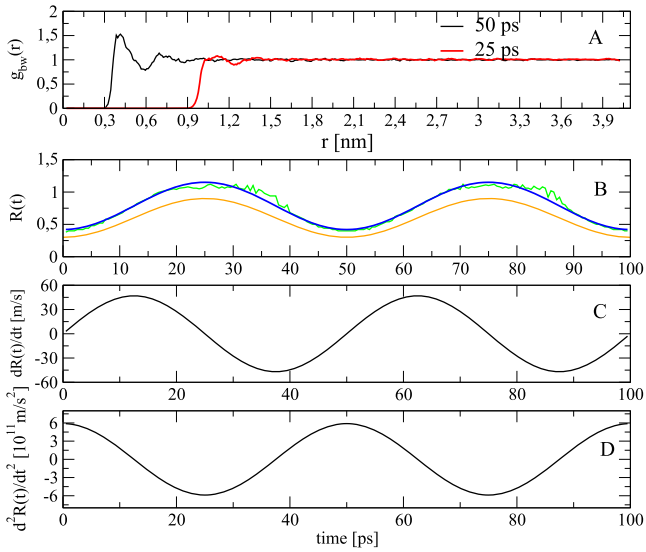

FIG. 1. (a) The radial distribution function $g_{\rm bw}$ between the bubble and oxygen atoms of waters when the bubble is fully expanded ($t = 25$ ps, red) and fully compressed ($t = 50$ ps, black). (b) Time-evolution of the bubble effective radius which is defined as the position of the first peak of $g_{\rm bw}$ (green) and its fitted curve (blue). The result of the predefined radius, Eq. (3), with $R_{\min} = 0.3$ nm and $R_{\min} = 0.9$ nm is shown in orange. (c) and (d) show the time-evolution of the bubble radius velocity and acceleration. Shown are results obtained for the cavitation with period $\tau = 50$ ps.

radius, and results displayed in Figs. 1(c) and 1(d) show that the bubble dynamics are rather complicated. Within the expansion phase ($t \leq 25$ ps), the bubble radius velocity increases initially from 0 to ~50 m/s, the acceleration decreases from 6×10^{12} m/s^2 to zero at 12.5 ps, and then the expansion is slowed down until the bubble reaches the maximum size at 25 ps, and therefore, during this time the acceleration is shown to be negative. After 25 ps, the bubble starts to be compressed with the magnitude of velocity increases to ~50 m/s at 37.5 ps before decreasing to zero when the bubble is fully compressed at 50 ps. Note that the velocity is negative in this phase because the motion is in the opposite direction with the expansion motion. This dynamical process is repeated during the stable cavitation.

B. Bulk water structure and hydrostatic pressure

Next, we wish to examine whether the cavitation induces any changes in bulk water. Here, bulk water is defined as all water molecules at distances D larger than 3 nm from the bubble center. We calculate the RDF between bulk water atoms $g_{\rm ww}(r)$ when the bubble reaches the minimum and maximum sizes. As seen from Fig. 2(a), $g_{\rm ww}(r)$ in both cases are virtually identical, with a low peak at $r \approx 0.2$ nm, corresponding to the hydrogen-oxygen interaction, and a higher peak at $r \approx 0.3$ nm, representing the oxygen-oxygen interaction. We then calculate the bulk pressure using the virial expression,

$$p = \frac{1}{3V_{\rm s}}\Big\langle \sum_{i=1}^{N_{\rm s}} [m_i \dot{\mathbf{r}}_i^2 + \mathbf{r_i}.\mathbf{F_i}] \Big\rangle, \tag{7}$$

where $\langle \cdots \rangle$ denotes the statistical average, $\mathbf{r_i}$ and $\mathbf{F_i}$ are the coordinate and the total force of the ith atom with mass m_i,

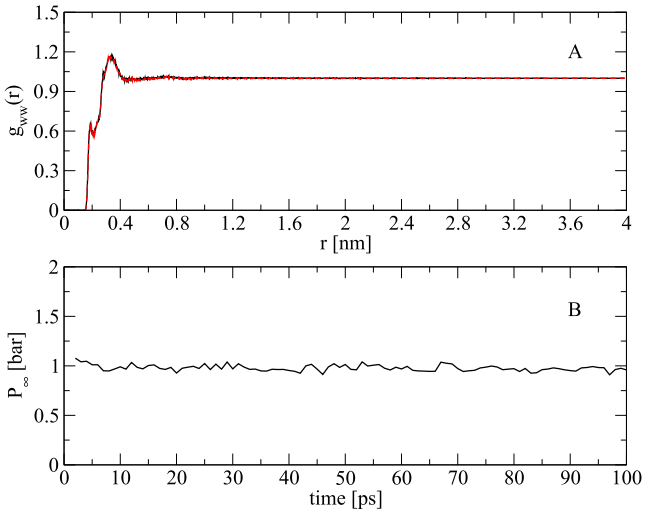

FIG. 2. (a) The radial distribution function between bulk water molecules when the bubble reaches the minimum (R_{min} = 0.3 nm, black) and maximum (R_{max} = 0.9 nm, red) sizes. (b) The time-evolution of the pressure of the bulk water during the bubble cavitation.

respectively. $V_s = 4\pi[(D + d)^3 - D^3]/3$ with the thickness d = 0.3 nm, accounting for the diameter of a water molecule and N_s is the number of water atoms in this volume. Here, we use the virial expression because there are many water molecules in the bulk, and thus, the statistical average is guaranteed. Figure 2(b) shows, as an example, the time-evolution of pressure of a slab of waters at the distance D = 4 nm from the bubble center, which is close to the box edge. As seen, the bulk water pressure is always stable around a reference value of ≈1 bar, despite the cavitation of the bubble. All together, these results show that the bulk water is hardly affected by the cavitation, and therefore, the assumption of constant hydrostatic pressure, p_∞, in the RP equation is valid in our simulations, and p_∞ = 1 bar is used in the calculation of the pressure using Eq. (5).

C. Verification of RP equation for a large amplitude of cavitation

In the following, we validate the RP equation for the case where the bubble undergoes a large amplitude (R_{min} = 0.3 nm, R_{max} = 0.9 nm) of cavitation with period τ = 50 ps.

1. Inner bubble pressure calculated from simulation data

We first calculate the inner pressure $p_g(R, t)$ from $g_{bw}(R, t)$. This function at a time step t during the cavitation is averaged over 100 trajectories. To reduce the statistical noise, we fit data points within the first solvation shell of $g_{bw}(R, t)$ to a function of the form

$$g(R,t) = \frac{e^{-(R(t)-\mu)^2/2\sigma^2}}{\sqrt{2\pi\sigma^2}}\left[1 + \mathrm{erf}\left(\xi\frac{R(t)-\mu}{\sigma}\right)\right], \qquad (8)$$

where μ, σ, and ξ are three fitted parameters. This functional form has been shown to be very accurate to fit to RDFs of fluids.[32] The height of the first peak is then calculated analytically from the maximization of Eq. (8), and the inner pressure is calculated from Eq. (6) and shown in Fig. 3 [(a), black curve].

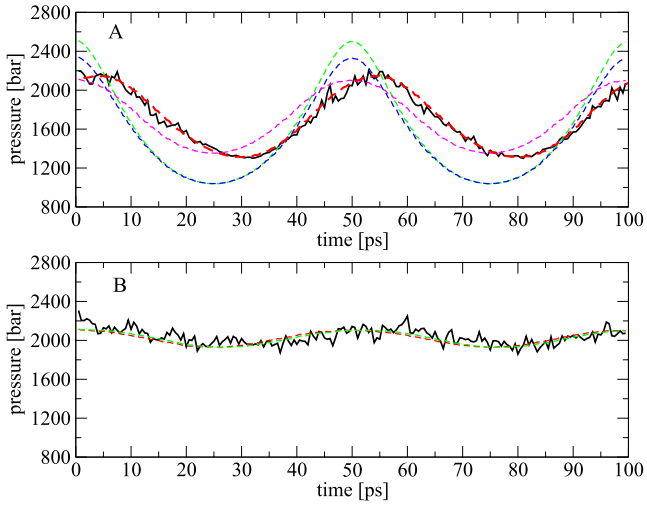

FIG. 3. (a) Time-evolution of the inner bubble pressure $p_g(R, t)$ during the stable cavitation with R_{min} = 0.3 nm and R_{max} = 0.9 nm. Shown are results calculated directly from simulation data (black) and from the RP equation with contribution from different terms: (i) γ_∞ = 49 mN/m, δ_T = 0 nm, and no viscosity (green), (ii) γ_∞ = 49 mN/m, δ_T = 0.045 nm, and no viscosity (blue), (iii) γ_∞ and δ_T are obtained from equilibrium simulations and no viscosity (magenta), and (iv) γ_∞ and δ_T are obtained from equilibrium simulations, $\eta_\infty = 2.91 \times 10^{-4}$ Pa s, and δ_{vis} = 0.67 nm (orange). (b) The same as panel (a) but for R_{min} = 0.3 nm and R_{max} = 0.4 nm with $p_g(R, t)$ is calculated from simulation (black) and predicted by the RP equation with: (i) γ_∞ and δ_T are obtained from equilibrium simulations, and no viscosity (red), and (ii) γ_∞ and δ_T are obtained from equilibrium simulations, $\eta_\infty = 2.91 \times 10^{-4}$ Pa s, and δ_{vis} = 0.67 nm (green). In all the cases, the period τ = 50 ps is used.

Following the bubble cavitation, the inner pressure oscillates between ~2205 bars when the bubble is fully compressed with radius R = 0.3 nm and ~1311 bars for the fully expanded bubble with R = 0.9 nm. Interestingly, we note that while the bubble reaches the maximum and minimum sizes at t = 25 and 50 ps, respectively, [Fig. 1(b)], the inner pressure reaches the minimum and maximum values about 5 ps later [Fig. 3(a)]. This is due to the solvent viscosity and will be discussed below.

2. Inner bubble pressure calculated by RP equation

Now, we calculate the pressure $p_g(R, t)$ using Eq. (5) considering the contribution of different terms. First, we calculate the last term, $\rho_0 V$, which represents the interaction between the bubble and a solvent molecule: $\rho_0 V = \rho_0\langle V_i\rangle$, where V_i is the Lennard-Jones interaction [Eq. (2)] between the bubble and the ith water molecule, and $\langle\cdots\rangle$ denotes the ensemble average over all waters within the first solvation shell around the bubble of 100 trajectories.

Second, let us consider the inertial term $I = \rho\{R\ddot{R} + 3\dot{R}^2/2\}$. It is calculated analytically using the analytical form of $R(t)$ and its time-derivatives, and the time-evolution is shown in Fig. 4. As seen, the behavior of the inertial term is rather complicated due to the complex behavior of both the velocity and acceleration, as shown in Figs. 1(c) and 1(d). Nevertheless, to explain qualitatively the positive and negative behaviors, we should note that the inertial can be considered as the work done by the bubble.[33] As shown above, during the first phase of bubble expansion the bubble radius velocity is increased, and this indicates that the inner bubble force is dominating over the solvent force, which tends to resist the

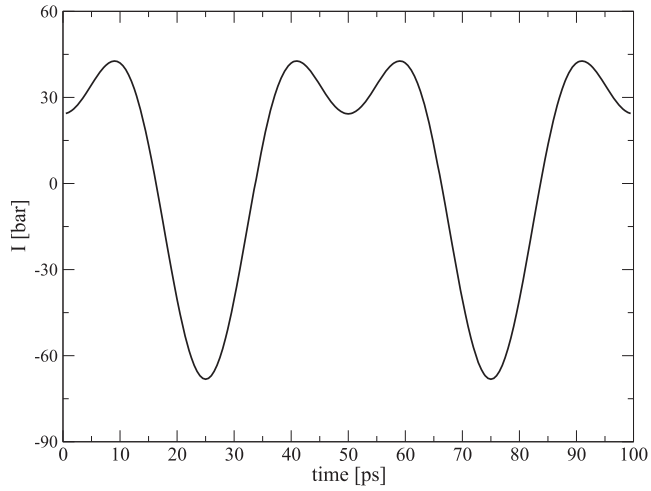

FIG. 4. Time-evolution of the inertial term $I = \rho\{R\ddot{R} + \frac{3}{2}\dot{R}^2\}$ during the bubble cavitation with period $\tau = 50$ ps, $R_{\min} = 0.3$ nm, and $R_{\max} = 0.9$ nm.

expansion. Because the bubble inner force points toward the solvent, the directions of the total force (sum of the inner and solvent forces) and bubble wall displacement must be the same, and this results in the positive work. In the second phase, the bubble is still expanded but slowed down, indicating that the solvent force is now dominating over the inner force. Thus, the directions of the total force and wall displacement are opposite, resulting in negative work. In any cases, the magnitude of the inertial term is quite small compared to the inner pressure, $p_g(R, t)$, shown in Fig. 3(a). This suggests that the inertial term plays a minor role in the RP equation.

Third, to study the effect of the bubble surface tension (third term), we exclude the contribution of the viscosity term (fourth term) but the first and last terms are included. We also ignore the curvature correction to the tension by setting $\delta_T = 0$ and consider the surface tension γ_∞ as a fitting parameter. A best fit of $p_g(R, t)$ data to Eq. (5) results in $\gamma_\infty = 49$ mN/m. This value is close to the bulk surface tension of the TIP3P water of 51 mN/m at $T = 300$ K and $P = 1$ bar.[34] However, the fitted curve shown in Fig. 3 [(a), green curve] deviates significantly from $p_g(R, t)$. A naive thinking could suggest us to consider the curvature correction coefficient to the tension, which should be important for sub-nano-sized bubbles. Taking $\gamma_\infty = 49$ mN/m and treating δ_T as a parameter, a best fit results in $\delta_T = 0.045$ nm. Overall, this value is in agreement with that obtained from the equilibrium measurement of the solvation energy of spherical cavities,[35] which is $\delta_T \approx 0.09$ nm. However, the fitted curve shown in Fig. 3 [(a), blue curve] still deviates from $p_g(R, t)$, except small improvements are obtained when the bubble reaches small sizes around 0, 50, and 100 ps.

Alternatively, we try to calculate the bubble surface tension from our equilibrium simulations. At equilibrium, Eq. (5) becomes

$$p_g^{\text{eq}}(R) = p_\infty + \frac{2\gamma(R)}{R} - \rho_0 V(R), \tag{9}$$

where the surface tension γ_∞ and its curvature correction coefficient δ_T are now absorbed into a size-dependent tension coefficient $\gamma(R)$ which is determined from equilibrium simulations as follows. We carry out 7 sets of equilibrium MD simulations where the bubble radii are fixed at $R = 0.3, 0.4, \ldots, 0.9$ nm. Each set consists of 100 trajectories, each 100 ps long, starting from the same initial structures used in NEMD simulations. The static RDFs between water molecules and the bubble are shown in Fig. 5(a). As usual, the peak of the RDF is high for small bubbles and becomes flat for larger bubbles. We should mention that in most simulations, a bubble is formed by removing some liquid molecules, creating an empty space in the liquid.[7,12–17,36,37] With this type of model, there is no interaction between the bubble and surrounding waters; therefore, the liquid density profile around the bubble surface is monotonic without peaks and its width has little size dependence.[7,36,37] By contrast, the peak seen in the RDF of our model is due to the interaction between the bubble and waters. The equilibrium inner pressure $p_g^{\text{eq}}(R)$ is calculated from the first peaks using Eq. (6) and shown in Fig. 5(b). The tension coefficient $\gamma(R)$ is then calculated for each bubble using Eq. (9) and shown in Fig. 5(c). As seen, the tension coefficient increases from 42 mN/m to 76 mN/m for bubbles with effective radii of 0.4 nm and 1.12 nm, respectively. Interestingly, the latter is quite close to the experimental value of 72 mN/m of the water-air surface tension at 1 bar and 300 K[38] but higher than the previous simulated value of 51 mN/m of the TIP3P water model.[34] Our higher value could be qualitatively understood because structural relaxation near the hard wall-water interface of our bubble model is more restricted than that near the free air-liquid interface.

Using the obtained equilibrium surface tension coefficients, we calculate $p_g(R, t)$ without the viscosity contribution, and the result is shown in Fig. 3 [(a), orange curve]. Obviously, the agreement between the pressures obtained by the RP equation and simulation is better now. However, we still observe a discrepancy, that is, the pressure in simulation changes slower than that calculated by the RP equation. For instance, the RP equation yields to the minimum and maximum pressures at 25 ps and 50 ps, respectively, while these values are obtained

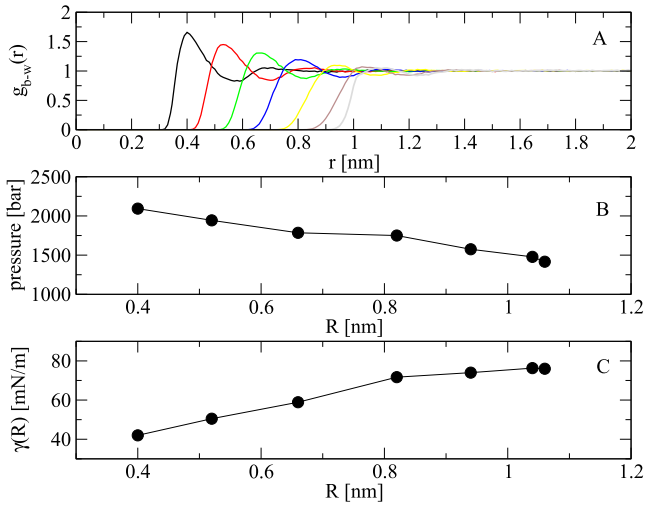

FIG. 5. (a) The radial distribution function between bubbles with different radii of 0.3, 0.4, . . ., 0.9 nm and water molecules. (b) The equilibrium inner bubble pressure $p_g^{\text{eq}}(R)$ as a function of the bubble radius calculated from the first peaks of the functions shown in (a). (c) The bubble surface tension as a function of the bubble radius calculated from pressures shown in (b) using Eq. (6).

at 30 and 55 ps in simulation. This suggests that the viscosity plays an important role in slowing down the bubble dynamics. Therefore, in the next step, we take into account the viscosity term in Eq. (5) by considering the bulk viscosity, η_∞, and the curvature correction coefficient $\delta_{\rm vis}$ as parameters. A fit of the $p_g(R, t)$ data to Eq. (5) (with the equilibrium surface tension) yields to $\eta_\infty = 2.91 \times 10^{-4}$ Pa s and $\delta_{\rm vis} = 0.67$ nm, and the fit is excellent as shown in Fig. 3 [(a), red curve]. The viscosity value differs only 10% from the TIP3P bulk value of 3.21×10^{-4} Pa s.[39] This could imply that the dispersion term which maintains our bubble does not alternate much the gas bubble dynamics. The same conclusion was also obtained by Dzubiella in the study of the collapse of a gas cavity in water.[7] We should mention that the calculated viscosity is much smaller than the experimental value of 8.96×10^{-4} Pa s, but this is a known problem of this water model and does not affect our results because the fitted viscosity η_∞ and the pressure $p_g(R, t)$ are consistently obtained from the same simulation using TIP3P water.

D. Verification of RP equation for a small amplitude of cavitation

Following the same procedure presented above, we now validate the RP equation for the small amplitude case with $R_{\rm min} = 0.3$ nm, $R_{\rm max} = 0.4$ nm, and period $\tau = 50$ ps. The inner pressure $p_g(R, t)$ is calculated directly from the simulation and shown in Fig. 3 [(b), black]. Due to the small amplitude of cavitation, the pressure only undergoes small changes between ~2205 bars and 1931 bars when the bubble is fully compressed and expanded, respectively. The maximum value of the inertial term is quite small ~−3.5 bar. We then calculate the inner pressure $p_g(R, t)$ [Eq. (5)] using the equilibrium surface tension [Fig. 5(c)] but without the contribution of the viscosity term, i.e., $\eta_\infty = 0$ Pa s and $\delta_{\rm vis} = 0$ nm. As seen from Fig. 3 [(b), green] the agreement between the RP pressure and its counterpart obtained from simulation data is very good. We should remind that without the viscosity, the RP pressure is not in good agreement with the simulation data for the large amplitude of cavitation case [Fig. 3(a)]. Next, we take into account the contribution of the viscosity by simply taking the values obtained from the large amplitude case, $\eta_\infty = 2.91 \times 10^{-4}$ Pa s and $\delta_{\rm vis} = 0.67$ nm, and calculating again the RP pressure. This only leads to a small improvement of the RP pressure [Fig. 3(b), green], suggesting that for a small amplitude of cavitation the viscosity plays a less important role.

IV. DISCUSSION

In the following, we focus the discussion on the assumptions that underline the RP equation, the finite-size effect, and the influence of the amplitude as well as the period of cavitation on the contribution of the inertial, surface tension, and viscosity terms of the RP equation.

A. Basic assumptions of RP equation

The first assumption of the RP equation is the incompressibility of the liquid. As seen from [Fig. 1(c)], the maximum velocity of the bubble radius is $\dot{R}(t = \tau/4) \sim 50$ m/s for the cavitation with $R_{\rm min} = 0.3$ nm and $R_{\rm max} = 0.9$ nm. Therefore, the Mach number, $\dot{R}(t)/c = 0.03$, is much smaller than unity, where the velocity of sound wave in water c is ~1500 m/s at the ambient temperature. We consider the Keller equation[40,41] which is a version of the RP equation where the compressibility is taken into account in the inertial term: $I^* = \rho\{(1 + \dot{R}/c)R\ddot{R} + 3(1 - \dot{R}/3c)\dot{R}^2/2\}$. The small value of the Mach number indicates that the Keller equation does not lead to any improvement in comparison to the RP equation, and the assumption of the liquid incompressibility of the RP equation is basically held.

The second assumption of the RP equation is the spherical deformation. We note that bubbles generated by initially heating or removing some liquid atoms as in previous cavitation simulations[7,12–15,36,37] are not necessary to be fully spherical, and thermal interface fluctuations during the cavitation may give rise to non-spherical instantaneous bubble shapes, thus theoretically violating the assumption of the RP equation. In our case, the interface is always maintained by a time-dependent Lennard-Jones potential between the bubble and surrounding waters, and the least square fit of the bubble radius data to the analytical form [Eq. (3)] results in a good fit as shown in Fig. 1, with the standard deviation less than 5%. This suggests that the bubble surface is more well maintained, but nevertheless will never be spherical symmetry due to fluctuations and the coarse nature of the solvent. Now, because the inner bubble pressure is calculated directly from the simulation data via RDFs [Eq. (6)], it must contain the surface deformation effect. Which terms in the RP equation can capture this effect? First, because the inertial term is calculated from the bubble radius, it must contain the surface deformation effect. However, as shown, the contribution of this term to the bubble pressure is very small; thus, the contribution of the deformation effect via this term is minor. Second, the surface tension and its curvature correction, $\delta_{\rm T}$, were calculated from equilibrium data; therefore, the surface deformation effect should already be taken into account. As shown, the viscosity and especially its curvature correction, $\delta_{\rm vis}$, are very important to describe correctly the bubble inner pressure, and this suggests that the effect of the surface deformation on the bubble pressure must be implicitly encoded in the curvature correction, $\delta_{\rm vis}$. Because the deformation is induced by the thermal interface fluctuations, we can therefore interpret $\delta_{\rm vis}$ as a correction to the curvature effect on the viscosity and capillary waves of the bubble surface.

B. Effects of finite-size, cavitation amplitude, and period on RP equation

Because the velocity and acceleration of the bubble radius depend on the ratio $\Delta R/\tau$ ($\Delta R \equiv R_{\rm max} - R_{\rm min}$) [Eq. (4)], it is sufficient to fix one parameter and study the influence of another parameter on the RP equation. In this study, we fix the period $\tau = 50$ ps and consider $\Delta R = 0.6$ nm and $\Delta R = 0.1$ nm. With these conditions, the inertial terms in both cases are small and their contribution to the inner pressure is minor for the stable cavitation. This result is consistent with that obtained by Dzubiella who showed that the inertial term is small,

although not completely negligible for the inertial cavitation of a bubble with an initial radius of 1.983 nm, but it is basically vanished for bubbles with radii ≤1 nm.[7] To quantitatively explain this, we calculate the Reynolds number $\mathcal{R} = \dot{R}(t)R(t)\rho/\eta_\infty$ with $\eta_\infty = 3.21 \times 10^{-4}$ Pa s being the bulk solvent viscosity of TIP3P water[39] and find that at the velocity $\dot{R} = 44$ m/s and radius $R(t) = 0.9$ nm the maximum value of $\mathcal{R}$ is 0.12, which is much smaller than unity, confirming that the inertial is indeed negligible, and the solvent friction dominates the bubble dynamics. However, we should note that this is not always true even for small bubbles undergoing small amplitudes of cavitation because as seen from the expression of the inertial term, it can be very large and contributes largely to the inner pressure, if the period τ is short. In this case, the liquid could be significantly disturbed and the hydrostatic pressure p_∞ is not necessary constant as in this study. In this case, the choice of p_∞ is very important. Indeed, Holyst and colleagues have studied an extreme case of cavitation where the bubble collapse is induced by traveling sound waves. If the constant ambient pressure is chosen, then a huge discrepancy between the RP equation and simulation was observed. However, when a pressure at the front of the waves is chosen, then the RP equation predicts correctly the collapse time of nano-bubbles.[14]

We note that the RP equation is derived for an infinite liquid medium; thus, it is theoretically not necessary to describe well simulation data, where the finite-size effect may suppress long-ranged hydrodynamics effects, and reduce the inertial.[42] To examine this problem from the simulation side, we carry out additional NEMD simulations with a larger box size of $L = 21$ nm, containing 188 354 waters, keeping the same other parameters. Surprisingly, the inner bubble pressure $p_g(R, t)$ calculated by the simulations of the small and large systems is almost identical (data not shown), suggesting that the finite-size effect in the simulation is probably negligible. To study this effect from the theoretical side, we employ the modified RP equation[43,44] which was developed for a confined liquid to calculate $p_g(R, t)$ from the RP equation [Eq. (5)]. The confinement effect is taken into account via the inertial term: $I_{\text{con}} = \rho\left\{R\ddot{R}(1-\lambda) + \dot{R}^2\left(\frac{3}{2} - 2\lambda + \frac{\lambda^4}{2}\right)\right\}$, where $\lambda \equiv R/R_c$ and $R_c = L/2$ is the radius of the confinement sphere. With the box length of $L = 7$ nm and maximum bubble radius of 1.12 nm, we obtain $\lambda \sim 0.25$, and the inertial term $I = \rho\{R\ddot{R} + 3\dot{R}^2/2\}$ in Eq. (5) is reduced by 25%. Given the fact that I is already small, the confinement effect is safely neglected in the RP equation, at least in our cases.

It has been suggested that viscous effects are important for bubbles with radii smaller than 10^{-3} m.[45] Our results show that the viscosity plays a major role in the dynamics of stable cavitation of nano-bubbles only if the velocity of cavitation is sufficient large, which is ∼50 m/s in our case. For small bubbles undergoing slow cavitation (with the velocity of ∼6 m/s in our case), then the viscosity may be negligible. Dzubiella has studied the inertial cavitation of an empty gas cavity in SPC/E water and found the collapse velocity of about ∼100 m/s. It is fast enough and therefore the viscosity together with the curvature correction coefficient δ_{vis} becomes important to describe correctly the bubble dynamics of inertial cavitation.[7] In contrast, Mao and Zhang have studied the collapse of an empty gas cavity in TIP3P water and obtained a negative surface tension, which implies the invalidity of the RP equation.[15] The authors attributed this artifact to the studied water model. However, from their result of the time-evolution of the bubble radius, we estimate the maximum collapse velocity of their bubble is about ∼160 m/s. Given this high velocity, we suggest that the absence of the viscosity term in their RP equation is the cause that leads to the negative surface tension. We note that Okumura *et al.* and Holyst *et al.* have shown that the collapse of a nano-bubble in the Lennard-Jones fluid is well described by the RP equation, although the viscosity is not included.[12,14] This is probably due to the fact that the viscosity is small and less important for Lennard-Jones liquid.[13]

Finally, to explain qualitatively the physics behind the contribution of the viscosity curvature correction, we note that the bubble reaches the maximum and minimum sizes at 25 and 50 ps, respectively [Fig. 1(b)]. However, as shown in Fig. 3(b), the bubble pressure reaches the minimum and maximum values around 5 ps latter. This delay must be caused by the liquid viscosity. Indeed, as shown above, to account for this shift, we must take into account the viscosity curvature correction δ_{vis} into the fit of the RP equation. This suggests that δ_{vis} is necessary to describe correctly the slowdown of the bubble cavitation. Now, it has been shown by Dzubiella and colleagues that for sub-nano-sized cavities (≤1 nm, as in our case) the diffusion of waters in the first solvation shell becomes slower than that in the bulk.[46] We believe that this slowed-down diffusion is the origin that induces the slowdown of bubble cavitation. Taken together, we suggest that the molecular physics of the viscosity curvature correction is to account for the anomalous behavior of the solvent around sub-nano-sized bubbles.

C. Implications for the applicability of RP equation in focused ultrasound modeling

As mentioned, the use of microbubbles coupled with ultrasound is emerging as a promising approach to open the blood-brain-barrier for drug delivery to treat brain diseases.[18] However, the molecular mechanism of the opening is still unknown. Because direct all-atom NEMD simulations of bubble cavitation under real experimental conditions are currently prohibited due to large system (μm) and long time (μs) scales, some mathematical modeling is employed. Basically, in this approach, parameters are taken from experiments and the RP equation is used to predict the dynamical pressure needed for the blood-brain-barrier opening.[20–25] Here, based on our results, we attempt to discuss the accuracy of the RP equation in the current mathematical modeling studies. In experiments, bubbles are much larger with the radii ranging from 0.5 to 4 μm and undergo a much slower vibration in size at frequencies ranging from 0.3 to 8 MHz (3333 - 125 ns).[47–50] Let us consider a typical case with $R_{\min} = 2$ μm, $\tau = 2$ MHz, and a relatively large amplitude of vibration of 0.5 μm. With these parameters, we obtain the largest inertial value $I = 0.25$ bar and largest cavitation velocity $\dot{R}(t) = 1$ m/s. We recall that in our study of the small amplitude of cavitation where the bubble radius varies between $R_{\min} = 0.3$ nm and $R_{\max} = 0.4$ nm, we obtain $I = 3.5$ bars and $\dot{R}(t) = 6$ m/s, which are much

larger than the above estimated values using experimental parameters. As shown above, the RP equation with the surface tension alone can predict accurately the bubble pressure for this slow cavitation case and thus also for the cavitation using experimental parameters. Furthermore, for micro-bubbles, the curvature correction to the surface tension is minor. Taken together, we argue that under conditions of the ultrasound-induced blood-brain-barrier opening experiments, the micro-bubble dynamics described by the RP equation depend insensitively on parameters; thus, the use of the RP equation in the current mathematical modeling studies of ultrasound-induced the blood-brain-barrier opening[20–25] should be sufficiently accurate.

V. CONCLUDING REMARKS

We have carried out NEMD simulations to verify, for the first time, the applicability of the RP equation in the description of stable cavitation of nano-bubbles. We have shown that this equation describes the bubble dynamics in liquid water quite well as long as the contributions of three terms, inertial, surface tension, and viscosity, are correctly taken into account. For subnano-bubbles ($\lesssim$1 nm) studied in this work, the contribution of the surface tension calculated, using the bulk water-air surface tension and its curvature correction, is not accurate, resulting in incorrect description of the RP equation. The inertial as well as the viscosity terms are directly and inversely proportional to the amplitude and period of cavitation, respectively. For small amplitudes and long frequencies, these terms are small and the surface tension term plays a major role in the RP equation. In contrast, large amplitudes and short frequencies yield fast cavitation velocity, therefore the viscous effect becomes important, and the curvature correction to bulk water viscosity must be considered, especially for subnano-bubbles. Due to very small bubble sizes, it is generally accepted that the inertial contribution is small. However, as shown above, this term may become very large if the period is short. In this case, the choice of the hydrostatic pressure in the RP equation is important to describe correctly the dynamics. We also show that the finite-size effect does not affect bubble dynamics obtained either from simulation or from the RP equation. In summary, our study together with previous studies[7,12–14] confirm that the RP equation is quite accurate to describe both stable and inertial bubble cavitation for nano-bubbles, although microscopic effects are not included in this equation. We also suggest that the use of the RP equation is quite accurate to model micro-bubble cavitation in the current theoretical modeling studies of the ultrasound-induced blood-brain-barrier opening experiments.

ACKNOWLEDGMENTS

This work has been supported by the Polish NCN Grant No. 2015/19/B/ST4/02721, CNRS, the National Science Foundation (NSF, Grant No. SI2-SEE-1534941), the National Institutes of Health (No. NIH-R01GM118508), the NC state HPC, and the IDRIS, CINES, TGCC centers for providing computer facilities (Project No. A0010707721).

[1] Lord Rayleigh, Philos. Mag. **34**, 94 (1917).
[2] M. S. Plesset, J. Appl. Mech. Trans. ASME **16**, 277 (1949).
[3] B. Noltingk and E. Neppiras, Proc. Phys. Soc. Sec. B **63**, 674 (1950).
[4] E. Neppiras and B. Noltingk, Proc. Phys. Soc. Sec. B **64**, 1032 (1951).
[5] P. Poritsky, in *Proceedings of the 1st US National Congress in Applied Mathematics* (ASME, 1952), p. 823.
[6] J. Dzubiella, J. M. J. Swanson, and J. A. McCammon, Phys. Rev. Lett. **96**, 087802 (2006).
[7] J. Dzubiella, J. Chem. Phys. **126**, 194504 (2007).
[8] T. G. Leighton, Ultrasonics **48**, 85 (2008).
[9] H. Lin, B. D. Store, and A. J. Szeri, J. Fluid Mech. **452**, 145 (2002).
[10] S. Putterman, P. G. Evans, G. Vazquez, and K. Weninger, Nature **409**, 782 (2001).
[11] V. E. Vinogradov, P. A. Pavlov, and V. G. Baidakov, J. Chem. Phys. **128**, 234508 (2008).
[12] H. Okumura and N. Ito, Phys. Rev. E **67**, 045301(R) (2003).
[13] R. Holyst, M. Litniewski, and P. Garstecki, Phys. Rev. E **82**, 066309 (2010).
[14] R. Holyst, M. Litniewski, and P. Garstecki, Phys. Rev. E **85**, 056303 (2012).
[15] Y. Mao and Y. Zhang, Nanoscale Microscale Thermophys. Eng. **17**, 79 (2013).
[16] F. Lugli, S. Hofinger, and F. Zerbetto, J. Am. Chem. Soc. **127**, 8020 (2005).
[17] F. Lugli and F. Zerbetto, ChemPhysChem **8**, 47 (2007).
[18] K. Hynynen, N. McDannold, N. Vykhodtseva, and F. A. Jolesz, Radiology **220**, 640 (2001).
[19] S. Ibsen, A. Tong, C. Schutt, S. Esener, and S. H. Chalasani, Nat. Commun. **6**, 8264 (2015).
[20] T. Nhan, A. Burgess, L. Lothar, and K. Hynynen, Phys. Med. Biol. **59**, 5987–6004 (2014).
[21] W. Wiedemair, Z. Tukovic, H. Jasak, D. Poulokakos, and V. Kurtcuoglu, Phys. Med. Biol. **57**, 1019 (2012).
[22] N. Hosseinkhah, D. E. Goertz, and K. Hynynen, IEEE Trans. Biomed. Eng. **62**, 1293 (2015).
[23] N. Hosseinkhah and K. Hynynen, Phys. Med. Biol. **57**, 785 (2012).
[24] N. Hosseinkhah, H. Chen, T. Matula, P. N. Burns, and K. Hynynen, J. Acoust. Soc. Am. **134**, 1875 (2013).
[25] S. Qin and K. W. Ferrara, Phys. Med. Biol. **51**, 5065 (2006).
[26] M. H. Viet, P. Derreumaux, and P. H. Nguyen, J. Chem. Phys. **145**, 174133 (2016).
[27] J. Takahashi and A. Morita, Chem. Phys. Lett. **573**, 35 (2013).
[28] E. Lindahl, B. Hess, and D. van der Spoel, J. Mol. Mod. **7**, 306 (2001).
[29] J. P. Ryckaert, G. Cicotti, and H. J. C. Berendsen, J. Comput. Phys. **23**, 327 (1977).
[30] T. Darden, D. York, and L. Pedersen, J. Chem. Phys. **98**, 10089 (1993).
[31] H. J. C. Berendsen, J. P. M. Postma, W. F. van Gunsteren, A. Dinola, and J. R. Haak, J. Chem. Phys. **81**, 3684 (1984).
[32] S. V. Sukhomlinov and M. H. Muser, J. Chem. Phys. **146**, 024506 (2016).
[33] C. E. Brennen, *Cavitation and Bubble Dynamics* (University Press, Oxford, 1995).
[34] C. Vega and E. de Miguel, J. Chem. Phys. **126**, 154707 (2007).
[35] D. M. Huang and D. Chandler, J. Phys. Chem. B **106**, 2047 (2002).
[36] G. Kikugawa, S. Takagi, and Y. Matsumoto, Comput. Fluids **36**, 69 (2007).
[37] Y. Matsumoto, J. Fluid Sci. Technol. **3**, 922 (2008).
[38] A. W. Adamson and A. P. Gast, *Physical Chemistry of Surfaces* (Wiley, New York, 1997).
[39] M. A. Gonzalez and J. L. F. Abascal, J. Chem. Phys. **132**, 096101 (2010).
[40] J. B. Keller and I. I. Kolodner, J. Appl. Phys. **27**, 1152 (1956).
[41] A. Prosperetti, Phys. Fluids **30**, 3626 (1987).
[42] B. Dunweg and K. Kremer, J. Chem. Phys. **99**, 6983 (1993).
[43] D. Obreschkow, P. Kobel, N. Dorsaz, A. de Bosset, C. Nicollier, and M. Farhat, Phys. Rev. Lett. **97**, 094502 (2006).
[44] T. Fourest, J. Laurens, E. Deletombe, and J. Dupas, Int. J. Impact Eng. **73**, 66 (2014).
[45] R. Chapman and M. Plesset, ASME J. Basic Eng. **93**, 373 (1971).
[46] R. G. Weiss, M. Heyden, and J. Dzubiella, Phys. Rev. Lett. **114**, 187802 (2015).
[47] N. McDannold, N. Vykhodtseva, and K. Hynynen, Ultrasound Med. Biol. **34**, 930 (2008).
[48] J. J. Choi, J. A. Feshitan, B. Baseri, S. Wang, Y. Tung, M. A. Borden, and E. E. Konofagou, IEEE Trans. Biomed. Eng. **57**, 145 (2010).
[49] G. Samiotaki, F. Vlachos, Y. S. Tung, and E. Konofagou, Magn. Reson. Med. **67**, 769 (2012).
[50] J. Choi, K. Selert, F. Vlachos, A. Wong, and E. E. Konofagou, Proc. Natl. Acad. Sci. U. S. A. **108**, 16539–16544 (2011).